CHEMISTRY OF MATERIALS
Article

*Chem. Mater.* **2010,** *22,* 5031–5041 5031
DOI:10.1021/cm101435s

# Novel Semiconductors Based on Functionalized Benzo[*d*,*d*′]thieno[3,2-*b*;4,5-*b*′]dithiophenes and the Effects of Thin Film Growth Conditions on Organic Field Effect Transistor Performance

Jangdae Youn,[†] Ming-Chou Chen,*[,‡] You-jhih Liang,[‡] Hui Huang,[†] Rocio Ponce Ortiz,[†,⊥] Choongik Kim,[†] Charlotte Stern,[†] Tarng-Shiang Hu,[§] Liang-Hsiang Chen,[§] Jing-Yi Yan,[§] Antonio Facchetti,*[,†] and Tobin J. Marks*[,†]

[†]*Department of Chemistry and the Materials Research Center, Northwestern University, 2145 Sheridan Road, Evanston, Illinois 60208-3113,* [‡]*Department of Chemistry, National Central University, Chung-Li, Taiwan 32054, ROC,* [§]*Industrial Technology Research Institute, Taiwan, ROC, and* [⊥]*Department of Physical Chemistry, University of Malaga, Malaga 29071, Spain*

*Received May 21, 2010. Revised Manuscript Received June 24, 2010*

A series of benzo[*d*,*d*]thieno[3,2-*b*;4,5-*b*]dithiophene (BTDT) derivatives, end-functionalized with phenyl (P) and benzothiophenyl (BT), were synthesized and characterized. A facile, one-pot synthesis of BTDT was developed which enables the efficient realization of a new BTDT-based semiconductor series for organic thin-film transistors (OTFTs). The crystal structure of P-BTDT was determined via single-crystal X-ray diffraction. Various combinations of dielectric surface treatment methods, substrate temperature, and deposition flux rate sequences have significant effects on device performance. Films deposited on octadecyltrichlorosilane (OTS)-treated $SiO_2$ substrates under properly adjusted substrate temperature and deposition flux rate achieve an efficaceous compromise between high film crystallinity and good film grain interconnectivity, resulting in good OTFT performance, with mobility greater than 0.70 $cm^2\ V^{-1}\ s^{-1}$ and $I_{on}/I_{off}$ greater than $10^8$.

## 1. Introduction

Over the past decade, organic semiconducting materials have been extensively developed for the fabrication of organic thin-film transistors (OTFTs), which have many potential applications in low-cost/printable electronics, such as flexible displays, Radio-frequency identification (RFID) components, and e-paper.[1−16] For recent reviews of this subject see refs 2 and 17−19. Among these materials, pentacene has attracted the greatest interest owing to its high performance, with typical field-effect mobilities of 0.5−1.0 $cm^2\ V^{-1}\ s^{-1}$.[20,21] Unfortunately, pentacene and several of its 6,13-functionalized derivatives suffer from rapid degradation in ambient conditions due to photoinduced oxidative decomposition and the formation of dimeric Diels−Alder adducts at the electron-rich central ring.[22−27] Therefore, sizable efforts have been devoted to improving pentacene stability by developing new heteroacenes with

*To whom correspondence should be addressed. E-mail: mcchen@ncu.edu.tw (M.-C.C.), a-facchetti@northwestern.edu (A.F.), t-marks@northwestern.edu (T.J.M.).

(1) Kim, C.; Facchetti, A.; Marks, T. J. *Science* **2007**, *318*, 76.
(2) Murphy, A. R.; Frechet, J. M. J. *Chem. Rev.* **2007**, *107*, 1066.
(3) Jones, B. A.; Facchetti, A.; Wasielewski, M. R.; Marks, T. J. *J. Am. Chem. Soc.* **2007**, *129*, 15259.
(4) Anthony, J. E. *Chem. Rev.* **2006**, *106*, 5028.
(5) Yan, H.; Chen, Z. H.; Zheng, Y.; Newman, C.; Quinn, J. R.; Dotz, F.; Kastler, M.; Facchetti, A. *Nature* **2009**, *457*, 679.
(6) Tang, M. L.; Mannsfeld, S. C. B.; Sun, Y. S.; Becerril, H. A.; Bao, Z. *J. Am. Chem. Soc.* **2009**, *131*, 882.
(7) Kobayashi, N.; Sasaki, M.; Nomoto, K. *Chem. Mater.* **2009**, *21*, 552.
(8) Marrocchi, A.; Seri, M.; Kim, C.; Facchetti, A.; Taticchi, A.; Marks, T. J. *Chem. Mater.* **2009**, *21*, 2592.
(9) Didane, Y.; Mehl, G. H.; Kumagai, A.; Yoshimoto, N.; Videlot-Ackermann, C.; Brisset, H. *J. Am. Chem. Soc.* **2008**, *130*, 17681.
(10) Subramanian, S.; Park, S. K.; Parkin, S. R.; Podzorov, V.; Jackson, T. N.; Anthony, J. E. *J. Am. Chem. Soc.* **2008**, *130*, 2706.
(11) Tang, M. L.; Reichardt, A. D.; Miyaki, N.; Stoltenberg, R. M.; Bao, Z. *J. Am. Chem. Soc.* **2008**, *130*, 6064.
(12) Ashizawa, M.; Yamada, K.; Fukaya, A.; Kato, R.; Hara, K.; Takeya, J. *Chem. Mater.* **2008**, *20*, 4883.
(13) Yagodkin, E.; Xia, Y.; Kalihari, V.; Frisbie, C. D.; Douglas, C. J. *J. Phys. Chem. C* **2009**, *113*, 16544.
(14) Ortiz, R. P.; Casado, J.; Hernandez, V.; Navarrete, J. T. L.; Letizia, J. A.; Ratner, M. A.; Facchetti, A.; Marks, T. J. *Chem.—Eur. J.* **2009**, *15*, 5023.
(15) Ortiz, R. P.; Facchetti, A.; Marks, T. J.; Casado, J.; Zgierski, M. Z.; Kozaki, M.; Hernandez, V.; Navarrete, J. T. L. *Adv. Funct. Mater.* **2009**, *19*, 386.
(16) Osaka, I.; Abe, T.; Shinamura, S.; Miyazaki, E.; Takimiya, K. *J. Am. Chem. Soc.* **2010**, *132*, 5000.
(17) Facchetti, A. *Mater. Today* **2007**, *10*, 28.
(18) Sirringhaus, H. *Proc. IEEE* **2009**, *97*, 1570.
(19) Arias, A. C.; Mackenzie, J. D.; McCulloch, I.; Rivnay, J.; Salleo, A. *Chem. Rev.* **2010**, *110*, 3.
(20) Kelley, T. W.; Boardman, L. D.; Dunbar, T. D.; Muyres, D. V.; Pellerite, M. J.; Smith, T. Y. P. *J. Phys. Chem. B* **2003**, *107*, 5877.
(21) Klauk, H.; Halik, M.; Zschieschang, U.; Eder, F.; Schmid, G.; Dehm, C. *Appl. Phys. Lett.* **2003**, *82*, 4175.
(22) Gao, J. H.; Li, R. J.; Li, L. Q.; Meng, Q.; Jiang, H.; Li, H. X.; Hu, W. P. *Adv. Mater.* **2007**, *19*, 3008.
(23) Yamada, H.; Yamashita, Y.; Kikuchi, M.; Watanabe, H.; Okujima, T.; Uno, H.; Ogawa, T.; Ohara, K.; Ono, N. *Chem.—Eur. J.* **2005**, *11*, 6212.
(24) Maliakal, A.; Raghavachari, K.; Katz, H.; Chandross, E.; Siegrist, T. *Chem. Mater.* **2004**, *16*, 4980.
(25) Coppo, P.; Yeates, S. G. *Adv. Mater.* **2005**, *17*, 3001.
(26) Meng, H.; Bendikov, M.; Mitchell, G.; Helgeson, R.; Wudl, F.; Bao, Z.; Siegrist, T.; Kloc, C.; Chen, C. H. *Adv. Mater.* **2003**, *15*, 1090.


Published on Web 08/04/2010

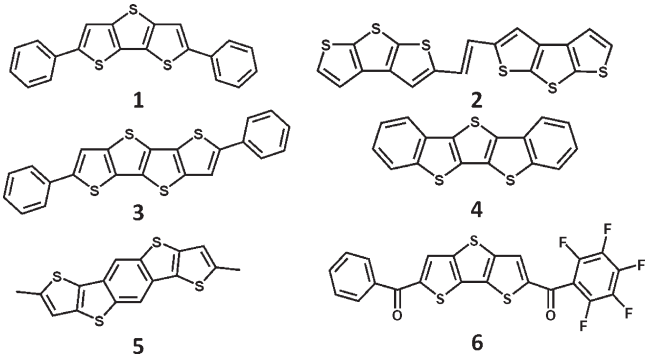

**Figure 1.** Examples of fused oligothiophene semiconductors used in OTFTs.

high charge carrier mobility. Fused thiophene-based materials have emerged as one of the most interesting alternatives due to their extensive conjugation, strong intermolecular S···S interactions, large band gaps, and high ambient stability. Several fused thiophene derivatives with the increased numbers of fused thiophene rings have been explored[28−31] (Figure 1) and have demonstrated moderate p-type charge transport performance. For example, compound **1**[28] and compound **2**[29] with three fused thiophene units and compound **3** with four fused thiophene units[31] exhibit hole mobilities up to 0.42, 0.89, and 0.14 $cm^2\ V^{-1}\ s^{-1}$, respectively. In addition, incorporating fused thiophene units into heteroacenes has proven to widen the highest occupied molecular orbital−lowest unoccupied molecular orbital (HOMO−LUMO) gap and energetically stabilize the HOMO level.[32,33] Five-ring fused pentacene analogs **4**[22] and **5**[34] exhibit hole mobilities of 0.51 and 1.7 $cm^2\ V^{-1}\ s^{-1}$, respectively. Furthermore, the first n-channel fused-thiophene material compound **6** with a mobility as high as 0.03 $cm^2\ V^{-1}\ s^{-1}$ has recently been reported.[35,36] Nevertheless, discovering new fused thiophenes with high thin-film transistor (TFT) performance and environmental stability, and thoroughly characterizing structure−property relationships remains an important task.

Along with synthetic efforts, the development of effective methods to optimize semiconductor film morphology is also critically important for optimizing OTFT performance. The film morphology of organic semiconductors depends on several important and poorly understood substrate/film growth parameters such as the gate dielectric surface characteristics, substrate temperature during film growth, and film deposition flux rate. The dielectric surface functionalization can change interfacial interactions between the gate dielectric and the semiconductor layer. Since charge transport takes place primarily within the first few semiconductor film monolayers at the dielectric−semiconductor interface,[37] device performance can be enhanced significantly by appropriate surface modification of the gate dielectric. One of the most effective surface treatment methods for $SiO_2$ gate dielectrics is via alkylsilane self-assembled monolayer (SAM) formation on the $SiO_2$ surface.[38] Indeed, acidic functional groups on the bare $SiO_2$ surface can act as charge traps, which can significantly decrease mobile charge carrier density and the OTFT performance. Organosilane SAM functionalization of the $SiO_2$ gate dielectric reduces the surface SiOH density, as well as decreases the surface energy of the $SiO_2$, which generally enhances the semiconductor film crystallinity.[39] At the initial stage of film growth, the adhesion between the $\pi$-cores of the adsorbate molecules and the substrate is much stronger than the adsorbate−adsorbate molecular adhesion strength.[40] As a result, the molecules at the interfacial region generally lie flat on the surface. SAM-functionalized surfaces with low surface energy reduce the adhesion strength between the adsorbate and the substrate, resulting in vertically aligned molecular orientations on the surface. For efficient transport of charge carriers, the $\pi-\pi$ stacking direction of the semiconductor molecules should ideally be in the same direction as the current flow. Therefore, silane SAM functionalization is instrumental in achieveing well-aligned $\pi-\pi$ conjugated films at the semiconductor−dielectric interface.

Another important molecular semiconductor film growth parameter is the substrate temperature since it determines the grain size in the semiconductor film. Polycrystalline films are composed of single crystalline grains and grain boundary regions, which play a critical role as charge traps.[41−44] Therefore, larger grains typically minimize the number of grain boundaries and charge traps. When the substrate temperature is increased, the semiconductor molecules diffuse more rapidly on the surface according to well-understood deposition kinetics.[45,46] Diffusing molecules are captured in islands since a potential barrier exists

(27) Kim, C.; Huang, P. -Y.; Jhuang, J. -W.; Chen, M. -C.; Ho, J. -Y.; Chen, L. -H.; Lee, G. -H.; Facchetti, A.; Marks, T. J. Org. Electron. **2010**, *11*, 1363.
(28) Sun, Y. M.; Ma, Y. W.; Liu, Y. Q.; Lin, Y. Y.; Wang, Z. Y.; Wang, Y.; Di, C. G.; Xiao, K.; Chen, X. M.; Qiu, W. F.; Zhang, B.; Yu, G.; Hu, W. P.; Zhu, D. B. *Adv. Funct. Mater.* **2006**, *16*, 426.
(29) Tan, L.; Zhang, L.; Jiang, X.; Yang, X. D.; Wang, L. J.; Wang, Z.; Li, L. Q.; Hu, W. P.; Shuai, Z. G.; Li, L.; Zhu, D. B. *Adv. Funct. Mater.* **2009**, *19*, 272.
(30) Liu, Y.; Di, C. A.; Du, C. Y.; Liu, Y. Q.; Lu, K.; Qiu, W. F.; Yu, G. *Chem.—Eur. J.* **2010**, *16*, 2231.
(31) Liu, Y.; Wang, Y.; Wu, W. P.; Liu, Y. Q.; Xi, H. X.; Wang, L. M.; Qiu, W. F.; Lu, K.; Du, C. Y.; Yu, G. *Adv. Funct. Mater.* **2009**, *19*, 772.
(32) Yamamoto, T.; Takimiya, K. *J. Am. Chem. Soc.* **2007**, *129*, 2224.
(33) Shinamura, S.; Miyazaki, E.; Takimiya, K. *J. Org. Chem.* **2010**, *75*, 1228.
(34) Gao, P.; Beckmann, D.; Tsao, H. N.; Feng, X. L.; Enkelmann, V.; Baumgarten, M.; Pisula, W.; Mullen, K. *Adv. Mater.* **2009**, *21*, 213.
(35) Chen, M. C.; Chiang, Y. J.; Kim, C.; Guo, Y. J.; Chen, S. Y.; Liang, Y. J.; Huang, Y. W.; Hu, T. S.; Lee, G. H.; Facchetti, A.; Marks, T. J. *Chem. Commun.* **2009**, *14*, 1846.
(36) Kim, C.; Chen, M. C.; Chiang, Y. J.; Guo, Y. J.; Youn, J.; Huang, H.; Liang, Y. J.; Lin, Y. J.; Huang, Y. W.; Hu, T. S.; Lee, G. H.; Facchetti, A.; Marks, T. J. *Org. Electron.* **2010**, *11*, 801.
(37) Dodabalapur, A.; Torsi, L.; Katz, H. E. *Science* **1995**, *268*, 270.
(38) Chua, L. L.; Zaumseil, J.; Chang, J. F.; Ou, E. C. W.; Ho, P. K. H.; Sirringhaus, H.; Friend, R. H. *Nature* **2005**, *434*, 194.
(39) Yang, H. C.; Shin, T. J.; Ling, M. M.; Cho, K.; Ryu, C. Y.; Bao, Z. *J. Am. Chem. Soc.* **2005**, *127*, 11542.
(40) Witte, G.; Woll, C. *J. Mater. Res.* **2004**, *19*, 1889.
(41) Pike, G. E.; Seager, C. H. *J. Appl. Phys.* **1979**, *50*, 3414.
(42) Orton, J. W.; Powell, M. J. *Rep. Prog. Phys.* **1980**, *43*, 1263.
(43) Horowitz, G. *Adv. Funct. Mater.* **2003**, *13*, 53.
(44) Tello, M.; Chiesa, M.; Duffy, C. M.; Sirringhaus, H. *Adv. Funct. Mater.* **2008**, *18*, 3907.
(45) Stadlober, B.; Haas, U.; Maresch, H.; Haase, A. *Phys. Rev. B* **2006**, *74*, 165302.
(46) Pratontep, S.; Nuesch, F.; Zuppiroli, L.; Brinkmann, M. *Phys. Rev. B* **2005**, *72*, 085211.

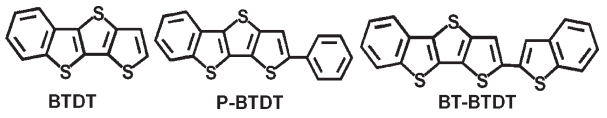


**Figure 2.** Chemical structures of the benzo[*d*,*d*′]thieno[3,2-*b*;4,5-*b*′] dithiophene (BTDT) semiconductors developed in this study.

at the edges of the islands, facilitating grain site growth. For this reason, films deposited at higher substrate temperatures typically exhibit large grain sizes, resulting in superior device performance if cracks do not form.[47,48]

Finally, the molecular deposition flux rate also appears to have a significant effect on film morphology. Grain growth kinetics can increase the size and depth of each grain boundary region. When films are grown slowly, molecules do not migrate to the lower layer but remain on top of islands, resulting in a 3D growth mode due to the potential energy barriers at the step edges. At slow deposition flux rates with low kinetic energy, the molecules cannot overcome the barrier at the step edges. Therefore, the semiconductor molecules do not completely fill the valleys between grains, resulting in large grain boundaries and voids. On the other hand, larger deposition fluxes can overcome the potential energy barriers for molecular diffusion at each grain boundary, and the molecules can reach the bottoms of the grain valleys. The outcome is a large density of nucleation sites with much smaller grain sizes. As a result, the interconnectivity between grains in the film is improved since large, deep grain boundaries are prevented. Therefore, several research groups have recently introduced a two-stage deposition technique to simultaneously maximize the film crystallinity and interconnectivity.[29,49] In this two-stage process, semiconductor films are initially grown at a very slow rate and, at a later stage, at a higher deposition rate. This combination of high crystallinity and good interconnectivity sometimes results in excellent charge transporting films.

In this contribution, we describe the facile synthesis of a new class four fused-ring heteroacene derivatives, based on the benzo[*d*,*d*′]thieno[3,2-*b*;4,5-*b*′]dithiophene (BTDT) core (Figure 2). In addition, molecular structure−property relationships are elucidated by introducing various functional groups on the BTDT core. Furthermore, film growth parameters relating to the $SiO_2$ gate dielectric surface treatment, the semiconductor film substrate temperature, and the molecular deposition flux rate are investigated to assess their effects on film microstructure and morphology. Our results reveal that TFTs based on phenyl benzo[*d*,*d*]thieno[3,2-*b*;4,5-*b*]dithiophene (P-BTDT) films deposited on octadecyltrichlorosilane (OTS)-treated substrates at 40 °C exhibit excellent p-channel mobilities up to 0.70 $cm^2\ V^{-1}\ s^{-1}$ and with good environmental stability. To the best of our knowledge, this is among the best device performance reported to date for four-ring fused thiophene organic semiconductors.

## 2. Experimental Section

**2.1. Materials and Methods.** All chemicals and solvents were of reagent grade and were obtained from Aldrich, Arco, or TCI Chemical Co. Reaction solvents (toluene, benzene, ether, and THF) were distilled under nitrogen from sodium/benzophenone ketyl, and halogenated solvents were distilled from $CaH_2$. $^1H$ and $^{13}C$ NMR spectra were recorded on a Bruker 500 or a 300 instrument. Chemical shifts for $^1H$ and $^{13}C$ NMR spectra were referenced to solvent signals. Differential scanning calorimetry (DSC) was carried out on a Mettler DSC 822 instrument, calibrated with a pure indium sample at a scan rate of 10 K/min. Thermogravimetric analysis (TGA) was performed on a Perkin-Elmer TGA-7 thermal analysis system using dry nitrogen as the carrier gas at a flow rate of 40 mL/min. The UV−Vis absorption and fluorescence spectra were obtained using JASCO V-530 and Hitachi F-4500 spectrometers, respectively, and all spectra were measured in the indicated solvents at room temperature. IR spectra were obtained using a JASCO FT/IR-4100 spectrometer. Differential pulse voltammetry experiments were performed with a CH Instruments model CHI621C electrochemical analyzer. All measurements were carried out at the temperature indicated with a conventional three-electrode configuration consisting of a platinum disk working electrode, an auxiliary platinum wire electrode, and a nonaqueous Ag reference electrode. The supporting electrolyte was 0.1 M tetrabutylammonium hexafluorophosphate ($TBAPF_6$) in a specified dry solvent. All potentials reported are referenced to a $Fc^+/Fc$ internal standard (at +0.6 V). Elemental analyses were performed on a Heraeus CHN-O-Rapid elemental analyzer. Mass spectrometric data were obtained with a JMS-700 HRMS instrument. Prime grade silicon wafers ($p^+$-Si) with ~300 nm (±5%) thermally grown oxide (from Montco Silicon) were used as device substrates.

**2.2. One-Pot Synthesis of Benzo[*d*,*d*′]thieno[3,2-*b*;4,5-*b*′]-dithiophene (BTDT).** Under nitrogen and anhydrous conditions at −78 °C, 2.5 M *n*-BuLi (21 mL in hexanes, 0.053 mol) was slowly added to an ether solution (30 mL) of 3-bromothiophene (5.1 mL, 0.053 mol), and the mixture was stirred for 40 min. This solution was then warmed to 0 °C under vacuum to remove $C_4H_9Br$, and then, ether (30 mL) was added. Note: without removing the *n*-$C_4H_9Br$, 3-butyl-*S*-thiophene is generated as a major side product after sulfur addition in the next step. At −78 °C, sulfur (1.68 g, 0.053 mol) was added to this ether solution, which was then stirred for 30 min, warmed to 0 °C, and stirred for another 30 min. Next, *p*-toluenesulfonyl chloride (TsCl, 10.62 g, 0.053 mol) was added to this solution at 0 °C; stirring was continued for 10 min, and then, the mixture was warmed up to 45 °C for 4 h. The reagent 3-Li-benzo[*b*]thiophene was prepared as in the above procedure from 2.5 M *n*-BuLi (19.1 mL in hexanes, 0.048 mol) and 3-bromobenzo[*b*]thiophene (10.2 mL, 0.048 mol, see preparation below). Again, this solution was warmed to 0 °C under vacuum to remove *n*-$C_4H_9Br$, and 40 mL of ether was added. At −78 °C, the second portion of 3-Li-benzo[*b*]thiophene ether solution was added to the first reaction mixture, stirred for 1 h, then warmed to room temperature, and stirred overnight. Next at 0 °C, 2.5 M *n*-BuLi (42.2 mL in hexanes, 0.105 mol) was slowly added to this mixture, which was stirred for 30 min, and then refluxed for 1 h. Next, $CuCl_2$ (15.4 g, 0.115 mol) was added to this mixture at 0 °C,

(47) Song, Y. B.; Di, C. A.; Yang, X. D.; Li, S. P.; Xu, W.; Liu, Y. Q.; Yang, L. M.; Shuai, Z. G.; Zhang, D. Q.; Zhu, D. B. *J. Am. Chem. Soc.* **2006**, *128*, 15940.
(48) Kalihari, V.; Tadmor, E. B.; Haugstad, G.; Frisbie, C. D. *Adv. Mater.* **2008**, *20*, 4033.
(49) Lee, H. S.; Kim, D. H.; Cho, J. H.; Park, Y. D.; Kim, J. S.; Cho, K. *Adv. Funct. Mater.* **2006**, *16*, 1859.

stirred for 1 h, warmed to room temperature, and stirred overnight. The resulting solids were collected by filtration, washed with water, extracted with benzene, and then chromatographed (silica gel; *n*-hexane as the eluent). The BTDT product was recrystallized from hexanes as a light-yellow powder to give a total of 3.85 g in a yield of 32%. $^1$H NMR ($CDCl_3$; 300 MHz): $\delta$ 7.86 (dd, $J$ = 7.8, 0.6 Hz, 1H), 7.82 (dd, $J$ = 7.8, 0.6 Hz, 1H), 7.42 (d, $J$ = 5.1 Hz, 1H), 7.38 (m, 2H), 7.34 (d, $J$ = 5.1 Hz, 1H). $^{13}$C NMR ($CDCl_3$; 300 MHz): $\delta$ 141.58, 141.49, 136.49, 133.51, 131.53, 129.51, 126.93, 124.88, 124.44, 123.90, 120.78, 120.61. MS (FAB) $m/z$: calcd for $C_{12}H_6S_3$, 246.3 ($M^+$); found, 246.3.

**2.3. Synthesis of 3-Bromobenzo[*b*]thiophene.**[50] At 0 °C, NBS (33.8 g, 0.19 mol) was added to a 400 mL THF solution of benzo[*b*]thiophene[51] (17.17 g, 0.13 mol), and the mixture was stirred for 0.5 h, then warmed to room temperature, and stirred for 36 h. Aqueous $Na_2S_2O_3$ solution was added next, and the desired product was extracted with ether and chromatographed (silica gel; hexanes as the eluent). The product was then further purified by distillation, giving a bright yellow oil, 25.9 g; yield, 95%. $^1$H NMR ($CDCl_3$): $\delta$ 7.85 (m, 2H), 7.45 (m, 3H). $^{13}$C NMR ($CDCl_3$; 300 MHz): $\delta$ 138.26, 137.18, 125, 124.74, 123.28, 122.75, 122.42, 107.51.

**2.4. Synthesis of 2-Phenylbenzo[*d*,*d*′]thieno[3,2-*b*;4,5-*b*′]dithiophene (P-BTDT).** Under nitrogen and anhydrous conditions at 0 °C, 2.5 M *n*-BuLi (0.49 mL in hexanes, 1.22 mmol) was slowly added to a 10 mL THF solution of BTDT (302 mg, 1.22 mmol), and the mixture was stirred for 40 min. Next, tri-*n*-butyltin chloride (0.38 mL, 1.35 mmol) was added, and the mixture was stirred for 30 min at this temperature, then warmed to room temperature, and stirred overnight. After simple filtration, THF was removed under vacuum, and 20 mL of toluene was loaded. The toluene solution was then transferred into a bromobenzene (0.14 mL, 1.35 mmol) and tetrakis (triphenylphosphine)palladium (57 mg, 0.049 mmol) toluene (10 mL) solution and was refluxed for 2 days. The desired solid product was collected by filtration, washed with hexanes and ether, and then purified by gradient sublimation at pressures of $\sim 10^{-5}$ Torr, giving a bright yellow solid, 182 mg; yield, 46%. $^1$H NMR ($CDCl_3$; 500 MHz): $\delta$ 7.88 (d, $J$ = 8 Hz, 1H), 7.83 (d, $J$ = 8 Hz, 1H), 7.67 (d, $J$ = 7.5 Hz, 2H), 7.58 (s, 1H), 7.44 (m, 3H), 7.35 (t, 2H). $^{13}$C NMR ($CDCl_3$; 500 MHz): $\delta$ 146.42, 142.37, 141.86, 136.20, 134.66, 133.72, 130.93, 130.02, 129.13, 128.11, 125.97, 125.07, 124.58, 124.03, 120.72, 116.74. Anal. Calcd for $C_{18}H_{10}S_3$: C, 67.04; H, 3.13. Found: C, 67.15; H, 3.02. HRMS (EI) $m/z$: calcd 321.9937 ($M^+$); found, 321.9945.

**2.5. Synthesis of 2-Benzothienylbenzo[*d*,*d*′]thieno[3,2-*b*;4,5-*b*′]-dithiophene (BT-BTDT).** At 0 °C, NBS (595.5 g, 3.31 mol) was added to a 100 mL THF solution of BTDT (816.3 mg, 3.31 mol), and the mixture was stirred for 0.5 h, then warmed to room temperature, and stirred overnight. Aqueous $Na_2S_2O_3$ solution was added next, and the desired 2-bromobenzo[*d*,*d*′]thieno[3,2-*b*;4,5-*b*′]dithiophene was extracted with $CH_2Cl_2$, chromatographed (silica gel; hexanes as the eluent), and recrystallized to give a bright yellow solid, 932.2 mg; yield, 89%.$^1$H NMR ($CDCl_3$; 300 MHz): $\delta$ 7.87 (d, $J$ = 7.8 Hz, 1H), 7.82 (d, $J$ = 7.8 Hz, 1H), 7.44 (t, $J$ = 7.5 Hz, 1H), 7.37 (d, $J$ = 7.5 Hz, 1H), 7.36 (s, 1H). $^{13}$C NMR ($CDCl_3$; 300 MHz): $\delta$ 141.42, 139.90, 135.72, 133.12, 131.78, 129.25, 125.06, 124.73, 123.95, 123.41, 120.72, 113.09. Under nitrogen and anhydrous conditions at 0 °C, 2.5 M *n*-BuLi (0.34 mL in hexanes, 0.85 mmol) was slowly added to a 10 mL THF solution of benzo[*b*]thiophene (114.3 mg, 0.85 mmol), and the mixture was stirred for 1 h. Next, tri-*n*-butyltinchloride (0.25 mL, 0.89 mmol) was added, and the mixture was stirred for 30 min at this temperature, then warmed to room temperature, and stirred overnight. After simple filtration, THF was removed under vacuum and 30 mL of toluene was added. The toluene solution was then transferred to a 2-bromobenzo[*d*,*d*′]thieno[3,2-b;4,5-*b*′]dithiophene (277.2 mg, 0.85 mmol) and tetrakis(triphenylphosphine)palladium (39.3 mg, 0.034 mmol) in toluene (20 mL) solution, and the mixture was refluxed for 2 days. The desired solid product was collected by filtration, washed with hexanes and ether, and then purified by gradient sublimation at pressures of $\sim 10^{-5}$ Torr, giving a bright yellow solid, 114 mg; yield, 35%. $^1$H NMR ($CD_2Cl_2$; 500 MHz): $\delta$ 7.89 (d, $J$ = 7.5 Hz, 1H), 7.85 (d, $J$ = 7.5 Hz, 1H), 7.7.83 (d, $J$ = 7.5 Hz, 1H), 7.77 (d, $J$ = 7.5 Hz, 1H), 7.59 (s, 1H), 7.51 (s, 1H), 7.46 (t, $J$ = 7.5 Hz, 1H), 7.39 (t, $J$ = 7.5 Hz, 1H), 7.37 (t, $J$ = 7.5 Hz, 1H), 7.33 (t, $J$ = 7.5 Hz, 1H). This material was insufficiently soluble to obtain a useful $^{13}$C NMR spectrum. Anal. Calcd for $C_{20}H_{10}S_4$: C, 63.46; H, 2.66. Found: C, 63.41; H, 2.72. HRMS (EI) $m/z$: calcd 377.9674 ($M^+$); found, 377.9665.

**2.6. X-ray Crystal Structure Determination of P-BTDT.** Yellow crystals suitable for X-ray diffraction were crystallized from a hot trimethylbenzene solution of P-BTDT. The chosen crystals were mounted on a glass fiber. Data collection for P-BTDT was carried out on a Bruker Smart Apex2 CCD diffractometer with Cu K$\alpha$ radiation ($\lambda$ = 1.54178 Å) at 100(2) K. After data collection, the frames were integrated and absorption corrections were applied. The initial crystal structure was solved by direct methods, the structure solution was expanded through successive least-squares cycles, and the final solution was determined. All of the nonhydrogen atoms were refined anisotropically. Hydrogen atoms attached to carbon atoms were fixed at calculated positions and refined using a riding mode. Crystal data, data collection, and refinement parameters are summarized in Table S1 (Supporting Information).

**2.7. OTFT Fabrication.** Thin film transistors were fabricated in a bottom gate-top contact configuration. Highly doped p-type (100) silicon wafers ( < 0.004Ω cm) were used as gate electrodes as well as substrates, and 300 nm $SiO_2$ thermally grown on Si was used as the gate insulator. The unit area capacitance is 10nF. The substrate surface was treated with octadecatrichlorosilane (OTS) or hexamethyldisilazane (HMDS), both purchased from Sigma-Aldrich Chemical Co. A few drops of HMDS were loaded inside a self-assembly chamber under an $N_2$ blanket. The $SiO_2$/Si substrates were exposed to this atmosphere for at least 7.0 days to give a hydrophobic surface. After HMDS deposition, the advancing aqueous contact angle is 95°. OTS was deposited under an $N_2$ blanket inside a self-assembly chamber. The $SiO_2$/Si substrates were exposed to an OTS toluene solution for 10 h to give a hydrophobic surface. After OTS deposition, the advancing aqueous contact angle of a water drop is 105°. Semiconductor thin films (50 nm) were next vapor-deposited onto the Si/$SiO_2$ substrates held at predetermined temperatures of 25 and 50 °C for P-BTDT and 25, 50, and 80 °C for BT-BTDT with a deposition rate of 0.1 Å/s at $6 \times 10^{-6}$ Torr, employing a high-vacuum deposition chamber (Denton Vacuum, Inc., USA). Gold source and drain electrodes (50 nm) were vapor-deposited at $2 \times 10^{-6}$ Torr through a shadow mask in the vacuum deposition chamber. Devices were fabricated with typical channel lengths of 50 and 100 $\mu$m and a channel width of 2000 $\mu$m.

**2.8. OTFT Characterization.** I−V plots of device performance were measured under vacuum, and transfer and output plots were recorded for each device. The current−voltage ($I-V$) characteristics of the devices were measured using a Keithley

(50) Marc, L.; Jeremie, F. D. C.; Lionel, J.; Emilie, D. *Tetrahedron* **2004**, *60*, 3221.
(51) Kashiki, T.; Shinamura, S.; Kohara, M.; Miyazaki, E.; Takimiya, K.; Ikeda, M.; Kuwabara, H. *Org. Lett.* **2009**, *11*, 2473.

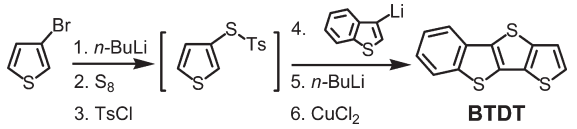


**Figure 3.** One-pot synthesis of the BTDT semiconductor core.

6430 subfemtoamperometer and a Keithly 2400 source meter, operated by a local Labview program and GPIB communication. Key device parameters, such as charge carrier mobility ($\mu$) and on-to-off current ratio ($I_{on}/I_{off}$), were extracted from the source-drain current ($I_{SD}$) versus source-gate voltage ($V_{SG}$) characteristics employing standard procedures. Mobilities were obtained from the formula defined by the saturation regime in transfer plots, $\mu = 2I_{SD}L/[C_iW(V_{SG} - V_T)^2]$, where $I_{SD}$ is the source-drain current, $V_{SG}$ is source-gate voltage, and $V_T$ is the threshold voltage. Threshold voltage was obtained from $x$ intercept of $V_{SG}$ vs $I_{SD}^{1/2}$ plots. Atomic force microscopy (AFM) measurements were performed using a JEOL 5200 Scanning Probe Microscope (JEOL Ltd. Japan) in the tapping mode.

**2.9. DFT Calculations.** Density functional theory (DFT) calculations on the present semiconductors were performed using the B3LYP funtional[52] and the 6-31G** basis set[53] as implemented in Gaussian 03 program. Vertical electronic excitation energies were computed using the time-dependent DFT (TDDFT) approach.[54,55] The 12 lowest energy electronic excitations were computed for all the molecules. TDDFT calculations were carried out using the B3LYP functional and the 6-31G** basis set on the previously optimized molecular geometries obtained at the same level of calculation.

## 3. Results and Discussion

**3.1. Synthesis.** The key building block of this semiconductor family is the new BTDT core (Figure 2), and therefore, a convenient, efficient, and inexpensive one-pot BTDT synthesis was developed. The synthetic route starts from inexpensive, commercially available materials, which do not require the expensive bis(phenyl-sulfonyl)sulfide, used in the published DTT synthesis.[56−58] As shown in Figure 3, 3-bromothiophene is first lithiated with *n*-BuLi, followed by $S_8$ and then by TsCl addition. Next, the mixture is treated with 3-lithiumthiophenylbenzene. Without product isolation, the crude mixture is subsequently dilithiated with *n*-BuLi and ring closure is achieved with $CuCl_2$ to afford BDTT in >32% yield. This simple route enables the synthesis of new asymmetric fused rings which are not accessible using previous fused-ring synthetic routes.[59]

The syntheses of functionalized BTDTs were achieved as shown in Figure 4. Deprotonation of BTDT with *n*-BuLi and then alkylstannylation affords the corresponding 2-BTDT-$SnR_3$ derivatives generated in situ, which are then coupled with the corresponding aryl bromide to give P-BTDT in ~46% yield, using a Stille coupling protocol. Since 2-benzothiophenyl tributyltin (2-BT-$SnR_3$) is easier to access than 2-benzothiophenyl bromide (2-BT-Br), BT-BTDT was prepared by coupling 2-BT-$SnR_3$ with 2-BTDT-Br in 35% yield (rather than 2-BT-Br + 2-BTDT-$SnR_3$).

**3.2. BTDT Derivative Thermal and Optical Properties.** Differential scanning calorimetry (DSC) data for BT-BTDT exhibit sharp endotherms above 258 °C, and thermogravimetric analysis plots reveal weight loss (~5%) only on heating above 255 °C (Table 1). The high melting temperatures of these new materials indicate excellent thermal stability. Lower melting points and lower weight loss temperatures are observed for BTDT derivatives with smaller molecular weights. The optical absorption spectra of compounds P-BTDT and BT-BTDT in $C_6H_5Cl$ solution (Figure 5) are significantly red shifted ($\lambda_{max} > 353$ nm) compared to that of the BTDT core ($\lambda_{max} \sim 315$ nm). Compared to phenyl-substituted P-BTDT, greater $\pi$-electron delocalization is observed for the benzothiophenyl derivative (BT-BTDT) giving the latter the lowest energy gap among the compounds in this series (Table 1). This result indicates substantial delocalization extending from the BTDT core to the substituents. Such delocalization is evident in Figure 6, where the computed topologies of the frontier molecular orbitals are depicted. As can be appreciated, both the highest occupied molecular orbital (HOMO) and the lowest unoccupied molecular orbital (LUMO) are fully delocalized over the entire $\pi$-conjugated skeletons for all the systems under study here.

To better understand the optical spectra, time-dependent DFT (TD-DFT) calculations were performed and the 12 lowest energy levels were estimated. These calculations are in very good agreement with the experimental data and predict that the electronic transitions having the highest oscillator strengths appear at 313, 354, and 389 for BTDT, P-BTDT, and BT-BTDT, respectively. These transitions can be assigned principally to monoelectronic HOMO to LUMO excitation. According to the topologies of these orbitals, the electronic transitions do not involve significant intramolecular charge transfer, which is also supported by the vibronic structure found in the optical spectra.

The HOMO−LUMO energy gaps calculated from the onset of the experimental optical absorption (2.99−3.44 eV) increase in the order of BT-BTDT < P-BTDT < BTDT. The same trend is found in the computational results, even if the theoretical HOMO−LUMO gaps are estimated to be somewhat larger (3.13−4.24 eV). These BTDT energy gaps are obviously larger than that of pentacene (1.77 eV). The larger optical bandgaps imply that these compounds are not easily oxidized and may have better stability in air. The photooxidative stability of the BTDT derivatives was also investigated by monitoring the absorbance decay at $\lambda_{max}$ of P-BTDT and

(52) Becke, A. D. *J. Chem. Phys.* **1993**, *98*, 1372.
(53) Francl, M. M.; Pietro, W. J.; Hehre, W. J.; Binkley, J. S.; Gordon, M. S.; Defrees, D. J.; Pople, J. A. *J. Chem. Phys.* **1982**, *77*, 3654.
(54) Gross, E. K. U.; Ullrich, C. A.; Gossmann, U. J. In *Density Functional Theory*; Gross, E. K. U., Dreizler, R. M., Eds.; NATO Advanced Study Institute Series B: Physics; Plenum: New York, 1995; Vol. *337*, pp 149−171.
(55) Chong, D. P. *Recent Advances in Density Functional Methods*; World Scientific: Singapore, 1995; p 115.
(56) Jong, F. D.; Janssen, M. J. *J. Org. Chem.* **1971**, *36*, 1645.
(57) Allared, F.; Hellberg, J.; Remonen, T. *Tetrahedron Lett.* **2002**, *43*, 1553.
(58) Frey, J.; Bond, A. D.; Holmes, A. B. *Chem. Commun.* **2002**, *20*, 2424.
(59) See Experimental Section for details.

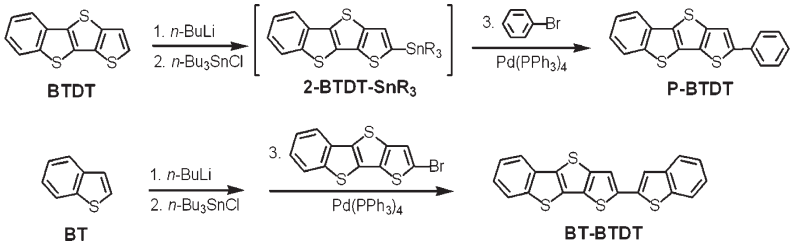


**Figure 4.** Synthetic routes to BTDT semiconductors.

**Table 1. Thermal, Optical Absorption/Emission, and Electrochemical Data for BTDT**

| compound | DSC $T_m$ (°C) | TGA (°C, 5%) | UV−vis[a] $\lambda_{max}$ (nm) | reduction potential (V)[b] | oxidation potential (V)[b] | $V_{gap}$ (eV) (optical)[a] | (DPV)[b] |
|---|---|---|---|---|---|---|---|
| BTDT | 175 | 175 | 315 | −1.89 | 1.5 | 3.44 | 3.39 |
| P-BTDT | 258 | 255 | 353 | −1.93 | 1.33 | 3.17 | 3.26 |
| BT-BTDT | 341 | 309 | 378 | −1.86 | 1.3 | 2.99 | 3.16 |

[a] in $C_6H_5Cl$. [b] by DPV in $C_6H_4Cl_2$ at 25 °C.

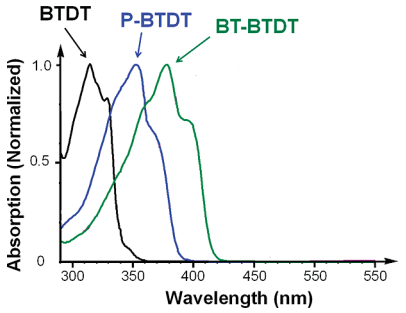


**Figure 5.** Optical spectra of BTDT derivatives in $C_6H_5Cl$ solution.

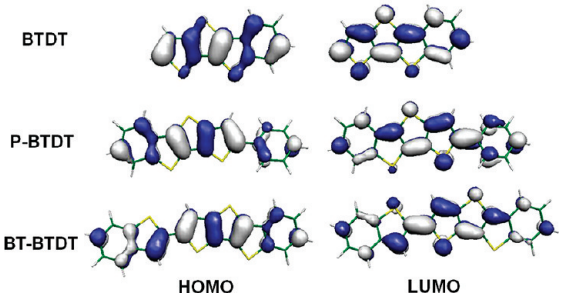


**Figure 6.** B3LYP/6-31G** electronic density contours for the frontier molecular orbitals of the molecules under study.

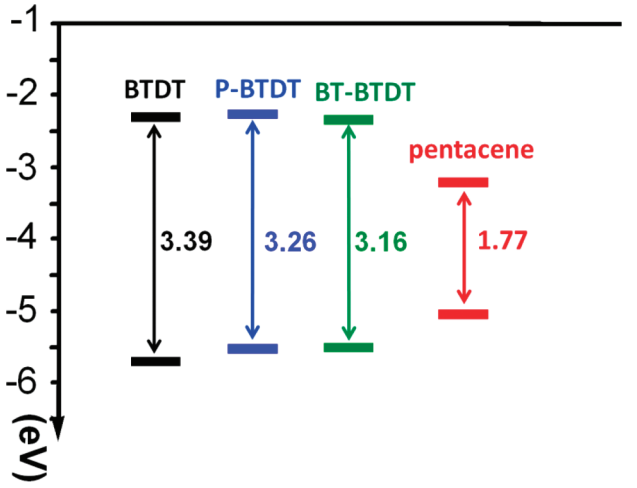


**Figure 7.** DPV-derived HOMO and LUMO energy levels of BTDT semiconductors.

BT-BTDT in aerated $C_6H_5Cl$ solutions exposed to the white light of a fluorescent lamp at room temperature. Under these conditions, no decomposition is observed after 4 to 5 days for any of these compounds, demonstrating the good stability of these materials.

**3.3. Electrochemical Characterization.** Differential pulse voltammograms (DPVs) of the present BTDT derivatives were recorded in dichlorobenzene at 25 °C, and the resulting reduction and oxidation potentials are summarized in Table 1. The DPV of P-BTDT exhibits an oxidation peak at +1.33 V and a reduction peak at −1.93 V (using ferrocene/ferrocenium as the internal standard at +0.6 V). As expected, the oxidation potentials of BT-BTDT ($E_{ox}$ = +1.30 V, $E_{red}$ = −1.86) are shifted to more negative values than those for P-BTDT, while the reduction potentials shift to less negative values, which can be attributed to the conjugative effects of the aryl substituents. The electrochemically derived HOMO−LUMO energy gaps obtained from the DPV data are ranked in the order of BT-BTDT (3.16 eV) < P-BTDT (3.26 eV) < BTDT (3.39 eV; Figure 7; assuming ferrocene/ferrocenium oxidation at 4.8 eV), which is consistent with the values obtained from optical spectroscopy: BT-BTDT (2.99 eV) < P-BTDT (3.17 eV) < BTDT (3.44 eV; Table 1). The electronically derived HOMO energy of the BTDTs is significantly lower than that of pentacene (−5.14 eV). The combination of the relatively low HOMO energies and large band gaps of BTDT series suggests that these are some of the most environmentally stable oligoacene semiconductors.

**3.4. Semiconductor Film Growth.** The TFT properties of P-BTDT and BT-BTDT were investigated on doped Si (gate)/$SiO_2$ (gate insulator) with several different gate dielectric surface treatments. Hexamethyldisilazane (HMDS)-modified substrates were prepared by exposing the Si/$SiO_2$ substrates to HMDS vapor for 7 days in a nitrogen atmosphere to yield a trimethylsilyl-coated surface. Octadecyltrichlorosilane (OTS)-modified substrates were fabricated by immersion of the Si/$SiO_2$ substrates in 3.0 mM dry toluene

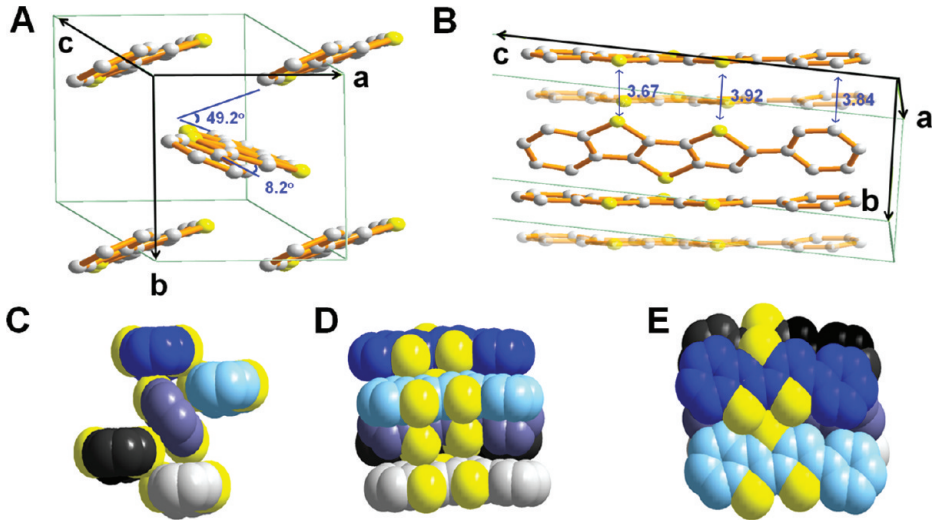


**Figure 8.** Crystal structure of P-BTDT. (A) Side view of the molecular stacking where the BTDT cores adopt an edge-to-face packing with a herringbone angle of 49.2°. (B) Front view and S−S/S−C/C−C/H−C distances in Å. (C, D, E) The side view, the front view, and the top view in space-filling models, respectively.

solutions of the silane reagent under nitrogen for 10 h. All substrates were characterized by advancing aqueous contact angle measurements, which indicate increasing hydrophobicity in the order of $SiO_2$ (< 5°), HMDS (97°), and OTS (104°). Additionally, the surface roughness was evaluated by tapping mode AFM, revealing a root-mean square (rms) roughness of 0.15 nm for $SiO_2$, 0.20 nm for HMDS, and 0.47 nm for OTS.

All semiconductor films (~50 nm thick) were vapor-deposited while maintaining the substrates at the temperatures ($T_d$) of 25, 50, 80, and 110 °C and with a deposition flux rate of 0.1 Å/s. For P-BTDT, an additional $T_d$ = 40 °C with two-stage deposition flux rates of 0.1 Å/s and 0.4 Å/s was also investigated. All films were characterized by $\theta$-$2\theta$ X-ray diffraction (XRD) and by tapping mode AFM.

**3.5. Single Crystal versus Polycrystalline Film XRD Analysis.** Before discussing the XRD results for the BTDT films, it is useful to begin by correlating film X-ray $\theta$-$2\theta$ scan data for the compound of known crystal structure. This initial study allows a much more thorough analysis of the molecular ordering in these compounds. The diffraction-derived single-crystal structure of P-BTDT is shown in Figure 8, and crystal structure determination data are summarized in the Supporting Information (Table S1).

Similar to other fused thiophenes,[22,28,29,31] the unit cell of P-BTDT exhibits the commonly observed herringbone packing motif (Figure 8A). The fused phenylene moiety is nearly coplanar with the three fused thiophenes, with a dihedral angle of 2.6°, while the dihedral angle between the phenyl moiety and the BTDT plane is 8.2°. P-BTDT molecules adopt an edge-to-face (herringbone) packing motif with an intermolecular packing angle of approximately 49.2°. The BTDT cores in P-BTDT are well aligned with the phenyl units packed on the same side (Figure 8B).[60] The shortest intermolecular S···C distance between the edge-to-face P-BTDT molecules is approximately 3.377 Å, with 3.665 Å for the shortest intermolecular S···S distance (Figure 8B). The molecular sheets are stacked along the *b*-axis direction and form a columnar array with an interplanar separation of 3.9 Å. Between the stacks, this interaction is reinforced by the close interplanar S···S contacts. In contrast, the theoretical calculations predict this molecule to be somewhat more twisted, with a dihedral angle between the phenyl ring and the BTDT moiety of ~25°. This disagreement may be explained by the fact that the calculations simulate an isolated molecule in vacuum while strong intermolecular interactions are clearly present in the crystal structure, which are not considered in the calculations.

With the crystal structure data in hand, it is straightforward to simulate the XRD powder pattern and, therefore, assign the reflections observed in the film XRD measurements (Figure 9).[61] The reflections from the simulated (random crystallite orientation) powder patterns that can be readily identified in the $\theta$-$2\theta$ scans and the $2\theta$ values of the experimentally observed reflections are summarized in Table 2. Figure 9 shows a typical graphical comparison of the experimental and simulated data, with a $2\theta$ scan for a P-BTDT film grown at $T_d$ = 40 °C on bare $SiO_2$ substrate and a P-BTDT powder pattern generated from the single-crystal data. The (0 0 *l*) reflection family is particularly pronounced, from (0 0 2) to (0 0 10). The (0 0 2) reflection in the film XRD is observed at $2\theta$ = 5.7°, corresponding to a *d* spacing of 15 Å (Table 2), approximately one-half the length of the unit cell *c* axis. This set of (0 0 *l*) reflections is predominant, even for P-BTDT films grown at room temperature (Figure S1A, Supporting Information). This indicates that the films are highly textured and that the P-BTDT molecules in the films

(60) Although the present molecule has an unusual unsymmetrical structure, no phenyl to fused phenylene ($C_6H_5$ to $C_6H_4$) $\pi-\pi$ stacking is evident in the crystal packing. Thus, apparently, the low symmetry of this molecule does not affect the crystallization arrangement.

(61) Facchetti, A.; Mushrush, M.; Yoon, M. H.; Hutchison, G. R.; Ratner, M. A.; Marks, T. J. *J. Am. Chem. Soc.* **2004**, *126*, 13859.

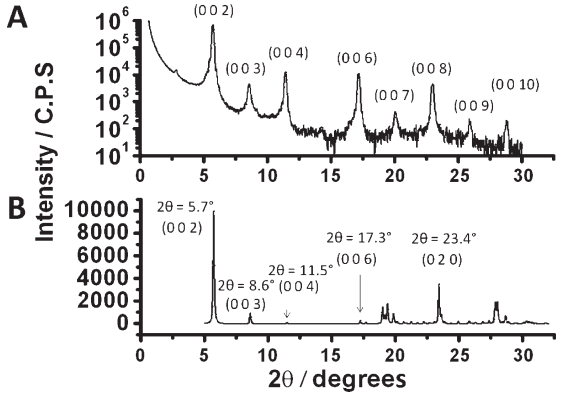


**Figure 9.** Comparison of the $\theta$-$2\theta$ XRD scan of a P-BTDT film grown at 40 °C on bare $Si/SiO_2$ (A) with the simulated powder pattern (B).

**Table 2. Thin Film X-Ray Diffraction Data for Semiconductors**

| compound | substrate temperature (°C) | $2\theta$ (deg) | $d$ spacing (A) (XRD) | (DFT cal.) |
|---|---|---|---|---|
| P-BTDT | 25, 50 | 5.69 | 15.5 | 15.1 |
| BT-BTDT | 25, 50 | 5.00 | 17.7 | 17.0 |

are predominantly aligned with their long molecular axes along the substrate normal; that is that film growth is favored in the $c$ direction. It is also apparent that higher deposition/annealing temperatures make this $c$-directional alignment even more favorable, as indicated by sharpening and increased intensity of the (0 0 $l$) reflections in the $\theta$-$2\theta$ scans of the corresponding films.

One question that arises is the absence in the $\theta$-$2\theta$ scans of reflection belonging to (0 k 0). The lowest observable reflections (0 2 0) would be observed at $2\theta = 23.42°$ according to the simulated powder diffraction pattern. This corresponds to $d$ spacing of 3.80 Å, approximately one-half of the unit cell $b$ axis. Although the (0 2 0) reflection is predicted in the simulated powder pattern to be intense, the absence of this peak in the film XRD of P-BTDT is likely due to the predominant ordering in the $c$ direction.

Over the entire $T_d$ range (25−50 °C), the P-BTDT films deposited on bare $SiO_2$ substrates exhibit reflections at the same values of $2\theta$ (Figure S1A, Supporting Information). As the deposition temperature is increased, the peaks become sharper, and their intensities increase with increasing $T_d$ (Figure S1A, Supporting Information). The consistency in reflection positions indicates the presence of a single polymorph and growth orientation across the $T_d$ range.[3] The increase in relative intensity of the higher order peaks on going from room temperature to higher growth temperatures indicates enhancements in the long-range order (Figure S1A, Supporting Information). The effect of surface treatment is relatively minor compared to the microstructural variation arising from different $T_d$s (Figure S2A, Supporting Information).

Although the single crystal structure of BT-BTDT was not determined, it is reasonable to assume that they have thin film microstructures similar to that of P-BTDT. Therefore, their peak orientations were assigned based on the simulated powder pattern extracted from the

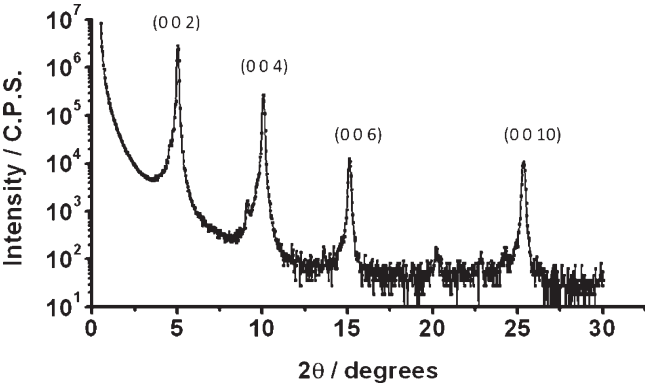


**Figure 10.** $\theta$-$2\theta$ XRD scan of a BT-BTDT film grown at 80 °C on a bare $Si/SiO_2$ substrates.

P-BTDT crystal structure. BT-BTDT thin films deposited at 80 °C on bare $Si/SiO_2$ exhibit only the family of (0 0 $l$) reflections (Figure.10). These data indicate good crystallinity of the film with long-range order. The (0 0 2) reflection in the film XRD is observed at $2\theta = 5.0°$, corresponding to a $d$ spacing of 17.7 Å (Table 2). This result is coincident with a computed molecular length of 17.0 Å from the DFT calculations. The fact that the calculated molecular length is so similar to the $d$ spacing from the thin film XRD data suggests that the orientation of molecules is almost perpendicular to the dielectric surface, providing an ideal $\pi-\pi$ stacking arrangement for charge transport. Furthermore, as $T_d$ is increased, the reflection intensities become more pronounced (Figure S1B, Supporting Information). The effect of the surface treatment is again relatively small when compared to microstructural variation with $T_d$s (Figure S2B, Supporting Information).

**3.6. Organic Thin Film Transistor Fabrication and Characterization.** Thin film transistors were fabricated in bottom gate-top contact configurations. Highly doped p-type (100) silicon wafers were used as gate electrodes as well as substrates, and 300 nm $SiO_2$ thermally grown on the Si was used as the gate insulator. Organic semiconductor thin films (50 nm) were vapor-deposited onto the $Si/SiO_2$, HMDS-treated, and OTS-treated substrates as described previously. Next, 50 nm gold source and drain electrodes were vapor-deposited at $2 \times 10^{-6}$ Torr through a shadow mask in a high vacuum deposition chamber. Devices were fabricated with typical channel lengths of 25, 50, and 100 $\mu$m, with a channel width of 2000 $\mu$m. Current−voltage ($I$−$V$) transfer and output plots were measured for each device under vacuum and in air. To illustrate the precision of each measurement, the reported data are an average of at least three devices tested at different regions of the semiconductor layer. Key device performance parameters, such as field-effect carrier mobility ($\mu$), threshold voltage ($V_T$), and on-to-off current ratio ($I_{on}/I_{off}$), were extracted using standard procedures.[62] The results are summarized in Table 3.

Since device parameters measured in air are statistically identical to those measured in vacuum, only the ambient

(62) Sze, S. M. *Physics of Semiconductor Devices*, 2 ed.; John Wiley & Sons: Hoboken, NJ, 1981.

**Table 3. Device Performance of BTDT Series**

| semiconductor | substrate temperature $T_d$ (°C) | surface treatment | air: mobility ($cm^2 V^{-1} s^{-1}$) | air: threshold voltage (V) | air: $I_{on}/I_{off}$ |
|---|---|---|---|---|---|
| P-BTDT | 25 | bare | 0.04 | −20 | $2.8 \times 10^7$ |
| | | HMDS | 0.04 | −23 | $1.4 \times 10^7$ |
| | | OTS | 0.07 | −29 | $3.3 \times 10^7$ |
| | 40 | bare | 0.02 | −20 | $6.3 \times 10^6$ |
| | | HMDS | 0.05 | −24 | $2.6 \times 10^7$ |
| | | OTS | 0.70 | −41 | $1.2 \times 10^8$ |
| | 50 | bare | NA[a] | | |
| | | HMDS | 0.07 | −22 | $1.2 \times 10^6$ |
| | | OTS | 0.11 | −22 | $7.6 \times 10^6$ |
| BT-BTDT | 25 | bare | 0.01 | −35 | $3.1 \times 10^5$ |
| | | HMDS | 0.02 | −36 | $2.2 \times 10^5$ |
| | | OTS | 0.01 | −33 | $1.2 \times 10^6$ |
| | 50 | bare | 0.01 | −32 | $5.3 \times 10^4$ |
| | | HMDS | 0.03 | −35 | $4.6 \times 10^5$ |
| | | OTS | 0.02 | −42 | $1.1 \times 10^5$ |
| | 80 | bare | 0.008 | −26 | $2.0 \times 10^6$ |
| | | HMDS | 0.02 | −31 | $1.8 \times 10^6$ |
| | | OTS | 0.02 | −19 | $6.6 \times 10^6$ |

[a] NA = not active.

results are presented in the table. Interesting insights can be drawn from these data. First, hydrophobic dielectric surface treatment, especially OTS treatment, yields the best p-type device performance. Second, TFT parameters including mobility ($\mu$) and on-to-off current ratio ($I_{on}/I_{off}$) are enhanced as the deposition temperature increases. Third, within the BTDT series, P-BTDT exhibits the best p-type TFT performance metrics with mobility = 0.70 $cm^2 V^{-1} s^{-1}$, threshold voltage ($V_{th}$) = −41 V, and on-to-off current ratio = $1.2 \times 10^8$ in air (Figure 11). This superior device performance is obtained by optimization of three different semiconductor film growth conditions: the gate dielectric surface treatment, $T_d$, and the film growth flux rate. Films deposited on OTS-functionalized substrates all afford the best device performance at the majority of the $T_d$s investigated. For P-BTDT, the mobility increases from 0.11 $cm^2 V^{-1} s^{-1}$ for semiconductor films deposited at $T_d$ = 25 °C to 0.70 $cm^2 V^{-1} s^{-1}$ for films deposited at $T_d$ = 40 °C.[63]

In order to better understand the electrical performance within this semiconductor series, intramolecular reorganization energies were estimated theoretically, using the DFT approach. The intramolecular reorganization energy ($\lambda$) describes the structural reorganization energetics required to accommodate delivered charges in transport. It consists of two terms associated with the geometric relaxation energies upon going from the neutral to the charged species and vice versa and is calculated directly from the adiabatic potential energy surfaces, as described elsewhere. (See details in Supporting Information, S3.)[64,65] In the present case, the reorganization energies are quite similar for all the semiconductors, 0.289 and 0.267 for P-BTDT and BT-BTDT, respectively. These values are larger than that reported for pentacene[66] (0.097 eV) or for other polycyclic benzene−thiophene structures[67] (0.118−0.204 eV) but are slightly smaller than that of pentathienoacene[68] (0.306 eV). From the theoretical results, it is apparent that neither trends in reorganization energies nor those in HOMO energies correlate with electrical performance. This argues that film morphological and microstructural characteristics rather than isolated molecule properties dominate TFT performance trends within this series of semiconductors.

**3.7. Semiconductor Film Morphology and TFT Performance.** The surface morphology of organic semiconductor thin films is often used to evaluate grain size and crystalline microstructure. The relevance of these data to TFT performance assumes that the surface microstructure is also characteristic of the thin film interface with the substrate/gate dielectric which is the active region for charge transport.[69] The highest carrier mobilities are obtained for films having the appropriate balance of large grain size and space-filling grain connectivity. The thin film morphology of BTDT films grown on different substrates was characterized by tapping-mode AFM, and the results highlight the effects of dielectric surface treatment, substrate temperature, and deposition flux rate. First, for all present semiconductors, the grain size increases when $T_d$ is increased. Second, although a hydrophobic surface usually results in large grains,[39] the trend is not obvious in the present BTDT family. Third, higher deposition flux rates produce smaller grains; however, the crystalline domains are well interconnected.

In the case of P-BTDT, films deposited on bare $SiO_2$ surfaces have a quite different film morphology compared with films deposited on alkyl silane SAM-treated surfaces (Figure 12A). Although the grain sizes are comparable to that on hydrophobic surfaces, the films deposited on bare $SiO_2$ exhibit larger voids between grains. The sizes of these void structures increase with the grain size when the films are deposited at higher substrate temperatures. For films deposited at 50 °C, the grains are disconnected, so that devices fabricated on these films do not exhibit measurable response (Table 3). If the poor film interconnectivity is the source of this low response, then device performance might be significantly improved by filling these voids with semiconductor. To test this hypothesis, the two-stage deposition method was introduced in this study. Thus, P-BTDT films were first deposited at 0.1 Å/s (10 nm) and next at

(63) Standard deviations between five data were < 20%.
(64) Malagoli, M.; Bredas, J. L. *Chem. Phys. Lett.* **2000**, *327*, 13.
(65) (a) Delgado, M. C. R.; Pigg, K. R.; Filho, D.; Gruhn, N. E.; Sakamoto, Y.; Suzuki, T.; Osuna, R. M.; Casado, J.; Hernandez, V.; Navarrete, J. T. L.; Martinelli, N. G.; Cornil, J.; Sanchez-Carrera, R. S.; Coropceanu, V.; Bredas, J. L. *J. Am. Chem. Soc.* **2009**, *131*, 1502. (b) Hutchison, G. R.; Ratner, M. A.; Marks, T. J. *J. Am. Chem. Soc.*, **2005**, *2339*, 16866.
(66) Coropceanu, V.; Malagoli, M.; da Silva, D. A.; Gruhn, N. E.; Bill, T. G.; Bredas, J. L. *Phys. Rev. Lett.* **2002**, *89*, 275503.
(67) Coropceanu, V.; Kwon, O.; Wex, B.; Kaafarani, B. R.; Gruhn, N. E.; Durivage, J. C.; Neckers, D. C.; Bredas, J. L. *Chem.—Eur. J.* **2006**, *12*, 2073.
(68) Kim, E. G.; Coropceanu, V.; Gruhn, N. E.; Sanchez-Carrera, R. S.; Snoeberger, R.; Matzger, A. J.; Bredas, J. L. *J. Am. Chem. Soc.* **2007**, *129*, 13072.
(69) Jones, B. A.; Facchetti, A.; Wasielewski, M. R.; Marks, T. J. *Adv. Funct. Mater.* **2008**, *18*, 1329.

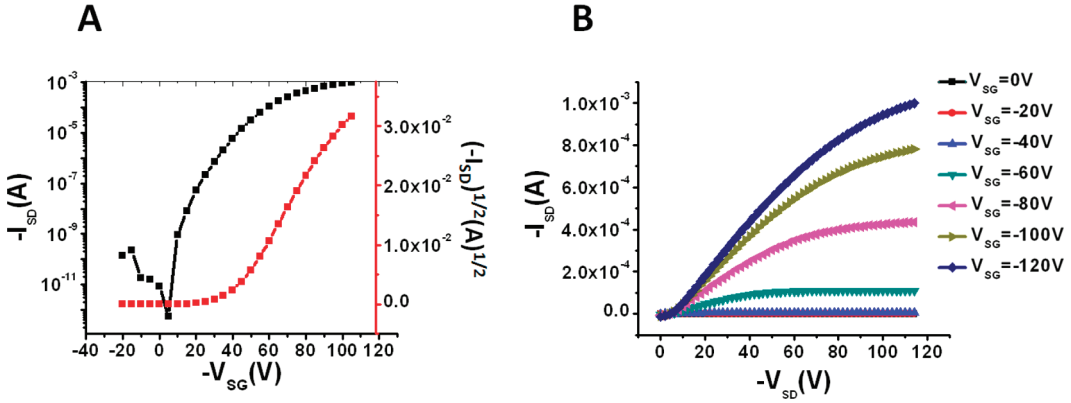


**Figure 11.** Transfer and output plots of an OFET device fabricated from P-BTDT films grown on an OTS-coated substrate: (A) transfer plot; (B) output plot. Substrate temperature = 40 °C, deposition flux rate = 0.1 Å/s, channel length = 25 $\mu$m, and channel width = 2000 $\mu$m. The device performance is as follows: $\mu$ = 0.70 cm$^2$ V$^{-1}$ s$^{-1}$, $V_{th}$ = −41 V, and $I_{on}/I_{off}$ = 1.2 × 10$^8$.

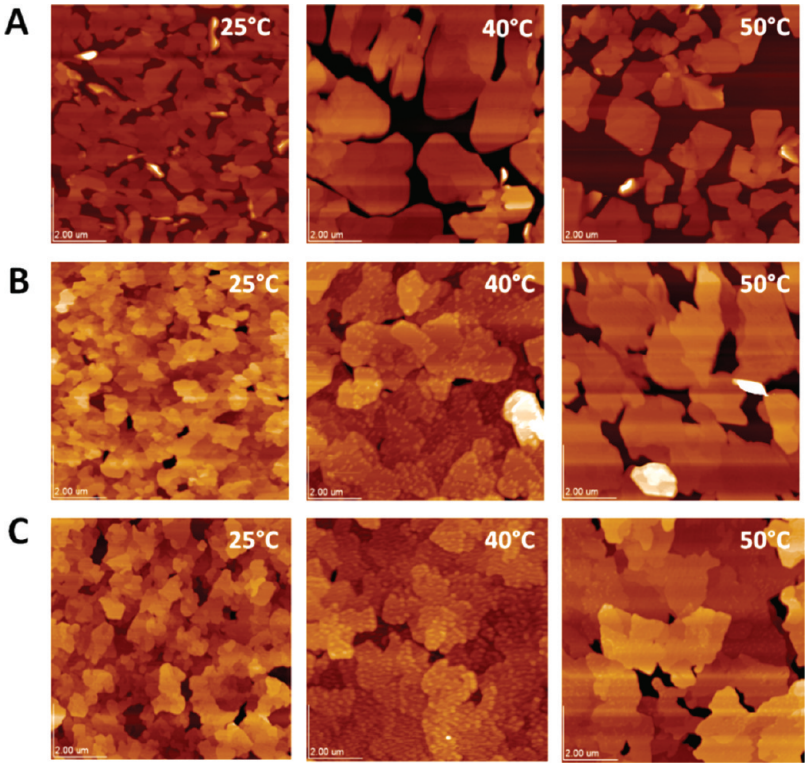


**Figure 12.** AFM images of P-BTDT films grown on different substrates and at different temperatures: (A) bare $SiO_2$, (B) $SiO_2$ with HMDS treatment, and (C) $SiO_2$ with OTS treatment (tapping mode, topography, 9 $\mu$m × 9 $\mu$m).

0.4 Å/s (40 nm) on bare $SiO_2$. As judged by AFM images, this approach significantly minimizes the grain boundary region in the semiconductor films (Figure 13).

Due to the enhanced film interconnectivity (Table 4), the TFT mobility increases from $\mu$ = 0.04 cm$^2$ V$^{-1}$ s$^{-1}$ to $\mu$ = 0.11 cm$^2$ V$^{-1}$ s$^{-1}$ for $T_d$ = 25 °C and from inactive to $\mu$ = 0.02 cm$^2$ V$^{-1}$ s$^{-1}$ for $T_d$ = 50 °C. Films on HMDS- and OTS-treated substrates have quite similar film morphologies (Figure 12B,C). P-BTDT is a representative example of the pronounced growth temperature sensitivity of film microstructure. Within a small deposition temperature range (25−50 °C), the film morphology changes significantly. As the substrate temperature increases, so does the grain size, and for $T_d$ = 50 °C, voids begin to appear in the film. The device performance degrades as a result. Films deposited on OTS at $T_d$ = 40 °C exhibit a good combination of large grain and film interconnectivity, resulting in TFTs exhibiting the highest performance metrics (Table 3).

BT-BTDT films deposited at 25 °C (Figure S3, Supporting Information) exhibit similar surface morphologies when grown on HMDS-treated and bare $Si/SiO_2$ substrates. Very large crystalline domains (> 3 $\mu$m) are observed in the films. However, the grain size of the BT-BTDT films on OTS-treated substrates is far smaller at all deposition temperatures. Considering that BT-BTDT TFT performance on all substrates is comparable, it is assumed that the smaller grain size observed on OTS is compensated by the well-connected film morphology. In addition, for all substrates, the mobility falls when $T_d$ is

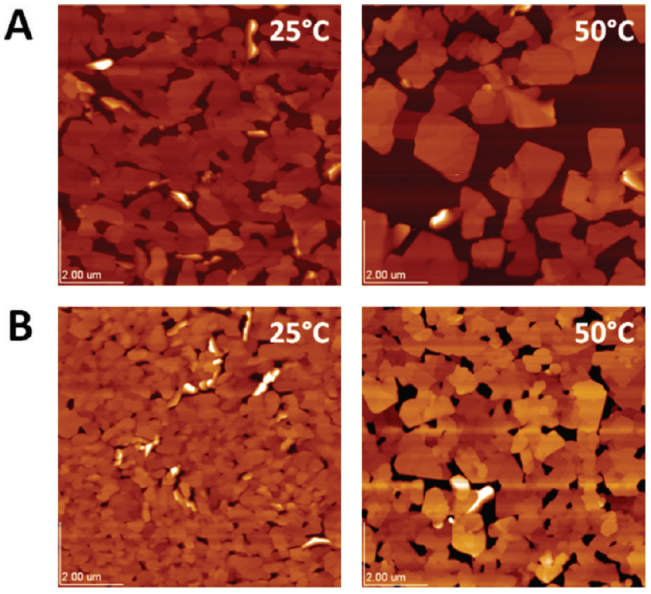


**Figure 13.** Comparison of AFM images of P-BTDT films grown on bare $SiO_2$: (A) slow deposition (50 nm film deposited at a growth rate = 0.1 Å/s) and (B) two-stage deposition process (10 nm at 0.1 Å/s, 40 nm at 0.4 Å/s; tapping mode, topography, 9 $\mu$m × 9 $\mu$m).

**Table 4. TFT Performance of P-BTDT Grown via Two-Stage Deposition**

| | | | air | | |
|---|---|---|---|---|---|
| compound | substrate temperature $T_d$ (°C) | surface treatment | mobility ($cm^2\ V^{-1}\ s^{-1}$) | threshold voltage (V) | $I_{on}/I_{off}$ |
| P-BTDT | 25 | bare | 0.11 | −29 | $2.9 \times 10^7$ |
| | | HMDS | 0.05 | −22 | $2.0 \times 10^6$ |
| | | OTS | 0.13 | −30 | $1.8 \times 10^7$ |
| | 50 | bare | 0.02 | −21 | $3.5 \times 10^6$ |
| | | HMDS | 0.07 | −31 | $5.7 \times 10^6$ |
| | | OTS | 0.12 | −31 | $2.9 \times 10^6$ |

increased from 50 to 80 °C. The size and depth of grain boundary regions in these highly crystalline films must have diminished the film interconnectivity.

**3.8. Shelf Life Test.** To monitor the stability of the present TFTs, shelf life tests for about 2 months were carried out. In agreement with the optical and thermal data, P-BTDT films are stable in air. After 2 months of shelf life in an ambient laboratory, P-BTDT-derived devices still exhibit $\mu = 0.3\ cm^2\ V^{-1}\ s^{-1}$ and $I_{on}/I_{off} = 10^7$.

## 4. Conclusions

A family of new benzo[*d*,*d*′]thieno[3,2-*b*;4,5-*b*′]dithiophene-based semiconductors was synthesized and characterized. TFT devices fabricated from these molecules exhibit good device performance with a good air stability. Various combinations of surface treatment methods, substrate temperature, and deposition flux rate sequences have significant effects on device performance. Films deposited on OTS-treated $SiO_2$ substrates under properly adjusted substrate temperature and deposition flux rate, achieve an efficacious compromise between high film crystallinity and good film grain interconnectivity, resulting in high OFET performance, with mobility greater than 0.70 $cm^2\ V^{-1}\ s^{-1}$ and $I_{on}/I_{off}$ greater than $10^8$. Further investigations on modifications of these molecules to better understand the structure/property relationships are currently underway.

**Acknowledgment.** We thank AFOSR (FA9550-08-01-0331) and the NSF-MRSEC program through the Northwestern Materials Research Center (DMR-0520513) for support of this research at Northwestern University. Financial assistance for this research was also provided by the National Science Council, Taiwan, Republic of China (Grant Numbers NSC98-2628-M-008-003, NSC97-2113-M-008-003, and NSC98-2627-E-006-003) and partially provided by Industrial Technology Research Institute of Taiwan under contract number ITRI 99-B-069351AA5130. R.P.O. acknowledges funding from the European Community's Seventh Framework Programme under Grant Agreement 234808.

**Supporting Information Available:** Table of crystal structure data for P-BTDT; $\theta$-$2\theta$ X-ray diffraction scans of P-BTDT and BT-BTDT films deposited at the indicated $T_d$ values and on the indicated substrates; reorganization energies; AFM images of BT-BTDT films grown on various substrates (PDF). This material is available free of charge via the Internet at http://pubs.acs.org.